Metformin-loaded Polymer-based Microbubbles/Nanoparticles Generated for the Treatment of Type 2 Diabetes Mellitus

Sumeyye Cesur[a,b], Muhammet Emin Cam[a,c,d], Fatih Serdar Sayın[e], Sena Su[a,b], Anthony Harker[f] , Mohan Edirisinghe[a,d] , Oguzhan Gunduz[a,g,*]

[a]Center for Nanotechnology & Biomaterials Application and Research (NBUAM), Marmara University, Turkey

[b]Department of Metallurgical and Materials Engineering, Institute of Pure and Applied Sciences, Marmara University, Turkey

[c]Department of Pharmacology, Faculty of Pharmacy, Marmara University, Istanbul 34668, Turkey

[d]Department of Mechanical Engineering, University College London, Torrington Place, London, WC1E 7JE, UK

[e]Department of Electrical and Electronical Engineering, Faculty of Technology, Marmara University, Turkey

[f]London Centre for Nanotechnology and Department of Physics & Astronomy, University College London, WC1E 6BT, UK

[g]Department of Metallurgical and Materials Engineering, Faculty of Technology, Marmara University, Turkey

ucemogu@ucl.ac.uk

Abstract

Type 2 diabetes mellitus (T2DM) is a chronic metabolic disease that is increasingly common all over the world with a high risk of progressive hyperglycemia and high microvascular and macrovascular complications. The currently used drugs in the treatment of T2DM have insufficient glucose control and can carry detrimental side effects. Several drug delivery systems have been investigated to decrease the side effects and frequency of dosage, to also increase the effect of oral antidiabetic drugs. In recent years, the use of microbubbles in biomedical applications has greatly increased and research into micro active carrier bubbles continues to generate more and more clinical interest. In this study, various monodisperse polymer nanoparticles at different concentrations were produced by bursting microbubbles generated using a T-junction microfluidic device. Morphological analysis by scanning electron microscopy, molecular interactions between the components by FT-IR, drug release by UV spectroscopy and physical analysis such as surface tension and viscosity measurement were carried out for the particles generated and solutions used. The microbubbles and nanoparticles had a smooth outer surface. When the microbubbles/nanoparticles were compared, it was observed that they were optimized with 0.3 wt.% polyvinyl alcohol (PVA) solution, 40 kPa pressure, and 110 µl /min flow rate, thus the diameters of the bubbles and particles were 100 ± 10 µm and 70 ± 5 nm, respectively. Metformin was successfully loaded into the nanoparticles in these optimized concentrations and characteristics, no drug crystals and clusters were seen on the surface. Metformin was released in a controlled manner at pH 1.2 for 60 min and at pH 7.4 for 240 min. The process and structures generated offer great potential for treatment of T2DM.

Keywords: Microbubble; nanoparticle; microfluidic device; drug delivery; metformin; diabetes mellitus

Introduction

Diabetes is a chronic disease that occurs when the pancreas can no longer make insulin or the body cannot use insulin well[1]. Heterogeneous aetio-pathology includes defects in insulin secretion, insulin action, or both, and disorders of carbohydrate, fat and protein metabolism. Diabetes has several pathological mechanisms. Irregularity of hepatic glucose metabolism is a major defect in the development of insulin resistance followed by Type 2 Diabetes Mellitus (T2DM)[2]. As reported by the report of World Health Organization, there will be at least 578 million people living with diabetes by 2030 [3] . Pharmacological agents currently used for the treatment of T2DM include oral anti-diabetic drugs, such as biguanides, sulfonylureas, and thiazolidinediones, have limited usage due to inefficacy in the progression of diabetic complications and undesirable side effects including nausea, hypoglycemia, liver, weight gain, diarrhea, and heart failure[4]. Present clinical guidelines recommend metformin as the first-line therapy for all newly diagnosed T2DM. As a biguanide, metformin is the most widely used oral anti-diabetic drug and suppresses hepatic gluconeogenesis and increases the sensitivity of hepatic insulin[5,6]. With oral administration of metformin, nearly 90% of the absorbed drug is eliminated renally within the first 24 hours. The plasma elimination half-life is nearly 6.2 hours, therefore, metformin is administered either two or three times per day[7]. Metformin can cause a important condition called lactic acidosis with symptoms such as tremors, dizziness, muscle pain, severe drowsiness, fatigue, blue / cold skin, fast / difficult breathing, slow / irregular heartbeat, nausea or vomiting, diarrheal stomach pain[8]. Several drug delivery systems have been investigated to decrease the side effects and frequency of dosage, to also increase the effect of oral antidiabetic drugs.

The use of microbubbles in applications such as the biomedical, cosmetic, food and chemical industries has gained significant importance in recent years, and research is ongoing on micro

active carrier bubbles[9–11]. Micro/nanoparticles containing biodegradable or biocompatible polymers are used for imaging, specific targeting and drug delivery in the treatment of a variety of diseases, such as cancer, diabetes, and tissue engineering[12–14].

There are different methods for preparing polymeric particles. Emulsion polymerization, solvent evaporation, coacervation, nanoprecipitation, spray drying, precipitation polymerization, phase separation, pressure spinning, electrohydrodynamic techniques can be used to produce microparticles in uniform size[15–18]**.** In previous work, metformin-loaded particles have been produced by these techniques. Metformin-loaded pectin nanoparticles[19], PLGA nanoparticles[20], alginate nanoparticles[21], chitosan nanoparticles[22], chitosan-capped nanoparticles[23], solid lipid nanoparticles[24] have been produced by different techniques in the recent years. Kumar et al. [25] loaded metformin into microcapsules coated with sodium alginate and gum karaya, drug release studies showed that microcapsules with controlled release properties have good mucoadhesive properties. Cao et al. [26] produced sustained release metformin HCl microcapsules using the Wurster-fluidized bed, and continuous release of metformin HCl from coarse microparticles of 213 μm was demonstrated. Cetin et al. [27] produced metformin HCl loaded nanoparticles by nanoprecipitation using Eudragit®RSPO polymer and Eudragit / PLGA polymer blend, all formulations showed high drug release profiles and *in vitro* drug release varied from 92 % to 100 % at 12 hours. However, these methods are not suitable for the production of uniform nanoparticles[28].

Microfluidics techniques have attracted attention recently because of their effectiveness in the production of micro / nanomaterials, and this technique is cost effective and can be used relatively easily because of its capabilities such as simple control of liquid flow and gas pressure[29,30]. Microfluidic devices allow microbubbles to be manufactured in a sole step and also have the potential to be used to produce multilayer coatings[31,32]. There are various types of devices that use microfluidic principles with different multiple intersections and flows. These

devices generate uniform size microbubbles and similar products due to continuous, reproducible and scalable manufacturing[33,34]. T-junctions and flow-focusing nozzles are some of the well-known methods with different device geometries used to produce microbubbles in microfluidic platforms [35,36]. The T-junction microfluidic device is one of the simplest methods of producing monodisperse and microbubbles at a high rate. Here the gas and polymer solution meet, a neck is formed and microbubbles begin to evolve [37]. The amount of delivered gas and the speed of the injector pump determines the size of the bubbles. In addition, the physical properties of the polymer solution, such as surface tension and viscosity, affect the bubble size. Natural and synthetic polymers can be used to produce micro and nanoparticle delivery systems[38]. Synthetic polymers are biocompatible, and can be biodegradable and absorbable. These materials play an important role in tissue engineering, drug delivery systems, and regenerative medicine[39]. Natural polymers have a structure that can be exploited in therapeutic applications, for example their non-toxic properties[40], and additional requirements can be input by carefuly selecting additives. They are used to produce biodegradable organic polymers such as polyvinyl alcohol (PVA) and sodium alginate (SA), nanocomposites and hydrogels for many biomedical applications[41]. PVA is a biocompatible polymer with many properties such as chemical stability, low toxicity, water solubility, good flexibility and excellent barrier properties. [42]. It is widely used due to its biocompatibility as part of biomedical and pharmaceutical applications such as drug delivery systems, contact lenses, artificial blood vessels [41,43]. In addition, PVA prevents agglomeration of the particle surfaces, resulting in a more monodisperse structure[44]. Biocompatible materials with the desired physical properties are obtained by mixing natural polymers with PVA[45]. SA is one of the most widely used biopolymers for nano/microparticle production and has biodegradable, biocompatible and mucoadhesive properties[46]. There are various advantages SA offers in numerous pharmaceutical and biomedical application such as drug delivery systems and cell

encapsulation [47,48]. Also, alginate-based materials are known to be sensitive to pH. This feature can be used for intelligent control of the release mechanism of encapsulated biomolecules from the alginate drug delivery carrier[49].

In this study, we explored combinations of different biopolymers such as PVA and SA. Thereafter, metformin-loaded microbubbles/nanoparticles were produced in the optimized polymer concentration using a T-junction microfluidic device. Polymeric nanoparticles were obtained in ideal properties such as a uniform shape, minimized size (~70 nm), and smooth outer surface by bursting microbubbles. The resulting structures offer significant potential for use in the treatment of T2DM, especially in drug delivery studies with nanoparticle forming ability.

Materials and Methods

Materials

Polyvinyl alcohol (PVA, Mw=89,000-98,000, 99% hydrolyzed), Sodium alginate (SA, Average molecular weight 216000 g/mol), and metformin were obtained from Sigma Aldrich, USA.

Preparation of Solutions

Polymeric solutions were prepared at various concentrations. PVA was dissolved in 10 mL distilled water at 90°C with magnetic stirring (Wise Stir®, MSH-20 A, Germany) for about 1 hour to obtain a solution consisted of 0.3 wt. % and 0.5 wt.% PVA. After 0.3 wt. % PVA and 0.5 wt. % PVA solutions reached room temperature (25°C), 0.5 wt. % SA was dissolved in this solution and this mixture was stirred for 20 min. Thereafter, 1 mg of metformin was added to the 3wt. % PVA (0.5 ml) solution for in vitro release study.

Characterization of Solutions

Density values were measured by using a standard 10 ml bottle. The surface tension of the solutions was measured using a force tensiometer Sigma 703D, Attention, Germany. The viscosity of solutions was determined using a DV-E, Brookfield AMETEK, USA instrument. All the measurements were carried out at ambient temperature (25 °C).

Microfluidic Device Design and Construction

A T-junction microfluidic device for producing the bubbles/particles was designed and constructed as shown in Figure 1. This microfluidic device was fabricated using poly(methyl methacrylate) (PMMA) by CNC machining and designed to resist high gas pressures. Teflon fluorinated ethylene polypropylene (FEP) capillaries with internal diameter (ID) = 100 μm and outer diameter (OD) = 1.6 mm were embedded in the PMMA block (dimensions: 22×27×15 mm).

Generation of Microbubbles

Teflon FEP tube was used to connect the inlets and outlet of the microchannels in the T-junction, which supplies gas and polymeric solutions. The vertical capillary of the T-junction device provided the gas exiting N_2 gas cylinder and it is connected to a manometer, which provides the necessary degree of control over the gas pressure. The other horizontal capillary channel allowed the flow of selected polymer solutions, and was fed and controlled using a 10 ml plastic syringe (Braun, Melsungen, GERMANY) connected to a digitally controlled syringe pump (NE-300, New Era Pump Systems, Inc., USA). After optimization of the processing conditions, both the polymeric solution and the gas met at the intersection region between the two capillaries, subsequently microbubbles were produced at the junction. Bubbles from the outlet channel were collected on glass slides or in the vials.

Bubble and Particle Characterization

An optical microscope (Olympus AnalySIS, USA) was used to examine the structure of the obtained microbubbles. All bubbles collected on the glass slides were allowed to dry in the oven at 25 °C for 24 hours. Morphological characterization of the dried samples was investigated using Scanning Electron Microscopy (SEM, EVO LS 10, ZEISS). Before imaging, the nanoparticles were coated by spraying with gold-palladium for 180 seconds using a Quorum SC7620 Mini Spray Coater. The applied acceleration voltage was 5 kV. In addition, the average bubble/nanoparticle diameter and distributions were measured using image software (Olympus AnalySIS, USA). Fourier-transformed infrared spectroscopy (FTIR) analysis was performed using a Jasco FT / IR-4700 model machine to examine the bonding structures and functional groups of pure PVA powder, metformin and metformin-loaded PVA nanoparticles. The measurements were taken at an average resolution of 4 cm^{-1} and 4000-400 cm.

Encapsulation Efficiency and Drug Release Study

The drug-loaded PVA nanoparticles (0.5 ml) were dissolved in 1 ml phosphate buffer (pH 7.4) at 37 ºC for 1 h under vigorous stirring. After completing this process, 1 ml of solution was taken and detected using a UV-visible spectrophotometer at 233 nm. The % encapsulation efficiency was calculated using the following equation:

$$\%EE = \frac{Wt}{Wi} \times 100$$

where Wt is the actual amount of drug in the nanoparticles and Wi is the quantity of drug added initially during nanoparticle generation. A series of standard solutions ranging from 2 to 10 µg/mL of metformin in distilled water was prepared and the absorbances were measured at 233 nm to draw the calibration curve.

Two samples of nanoparticles containing 1 mg drug (0.5 ml) were collected into Eppendorf tubes and 1 ml PBS solution (1.2 pH and 7.4 pH) were added on each sample. The release of

metformin from 0.3 wt.% PVA nanoparticles samples was performed in both 1.2 and 7.4 phosphate buffer solutions in a shaking incubator (37 ºC, 200 rpm). At determined time intervals, 1 ml solution was collected from the tubes and the amount of drug release was measured at 233 nm by UV-Vis spectrophotometer. Then an equal amount of fresh PBS solutions were added again to maintain the original volume. Each experiment was carried out in triplicate.

In vitro Release Kinetics

To investigate the drug release mechanisms and metformin release profiles from microbubbles four equations; zero order, first order, Higuchi, and Korsmeyer-Peppas equations, were considered, as represented in Eqns. 1–4.

$$Q = \min(K_0 t, 1) \quad (1)$$

$$\ln(1 - Q) = -K_1 t \quad (2)$$

$$Q = \min(K_h t^{1/2}, 1) \quad (3)$$

$$Q = K t^n \quad (4)$$

where Q is the fractional amount of drug release at time t; K_0, K_1, K_h and K are the kinetic constants for zero order, first order, Higuchi, and Korsmeyer-Peppas models, respectively. n is the Korsmeyer-Peppas release exponent, which is indicative of the drug release mechanism. As there are too few points on the release curve below 60% release to make meaningful deductions from the Korsmeyer-Peppas model we have instead used the expression(62)

$$Q = \tanh(K t^{1/2}), \quad (5)$$

in which the parameter *K* may be related to the diffusion coefficient of the drug in a spherical particle. Equation (5) is based on Fickian diffusion out of a sphere, but is applicable across the whole release profile. All the expressions may be generalised to include the maximum release fraction as an additional parameter, but this does not affect our main conclusions.

Results and discussion

In this study, diverse monodisperse polymeric and drug loaded nanoparticles were produced with bursting microbubbles using a T-junction device. Changing the bubble size can affect the particle size [28]. The two different components consisting of the liquid and gas phases from two independent supply channels intersect in the mixing area of the microfluidic device. Because of their density differences, the polymer mixture is encapsulated by gas bubbles. Under the influence of gas pressure, the outlet is expelled through the capillary. As a result of the continuous flow of bubbles, a cloud of bubbles are generated at the outlet. The dimensions and shapes of these bubbles vary depending on the different geometric orifices in the gas/liquid intersection region and fluctuations in the outlet of the gas source[28,50,51].

In addition, surface tension and viscosity are two important solution properties that affect the formation of monodisperse microbubbles/particles. These are the dominant factors in microfluidic systems[37,52]. The physical characterics of the polymer solutions are shown in Table 1. The surface tensions of 0.3wt.%, 0.5 wt.% PVA and 0.5wt.% (PVA-SA) solutions in distilled water are 42.9 mN / m, 42.4 mN/ m, and 44.9 mN / m, respectively. As the PVA concentration increased from 0.3wt. % to 0.5wt. %, the surface tension values of the solutions decreased. In a study by Bozic et al. [53], surface tension values decreased up to 0.5 wt.%. PVA concentration. After this point, surface tension increased as the PVA concentration increased. The surface tension value was slightly increased by adding 0.5wt.% SA to the solution containing 0.5wt.% PVA. It was also observed that the viscosity of the solutions increased with increasing polymer concentration. The viscosity increased from 286 to 330 mPa.s as the PVA concentration

increased from 0.3wt. % to 0.5wt.%. Furthermore, the viscosity increased when 0.5wt. % SA was added to 0.5wt. % of PVA solution[54]. With the addition of metformin to 0.3 wt. % PVA solution, the surface tension and viscosity increased to 43.0 mN / m and 290 mPa.s, respectively.

Furthermore, the size of the microbubbles produced varies depending on the flow rate of the polymer solution and the pressure of the gas source[49]. Three different solutions at different concentrations were prepared for the production of microbubbles. One of these, 0.5wt.% PVA solution was injected from inlet I (Figure 1). At the same time, N_2 gas was pumped through the inlet II in Figure 1. The constant gas pressure was applied with a flow rate of 90 µl / min to form microbubbles. To produce the smallest and monodisperse microbubbles, the solution flow rate was changed and increased from 90 to 110 µl/min while maintaining a constant gas pressure of 70 kPa. As shown in the optical microscope images of the microbubbles in Figure 2A, the average microbubble diameter decreased from 267 ± 32 µm to 250± 45 µm when the solution flow rate was increased from 90 µl / min to 110 µl / min at a constant gas pressure of 70 kPa. Increasing the flow rate at constant pressure reduces the bubble size[37].

Explosion-like disintegration occurs with the release of N_2 gas in these microbubbles [55]. Spherical solid PVA nanoparticles are formed simultaneously. According to the micrographs in Figure 2B, the diameter distributions of 0.5 wt.% PVA nanoparticles are 205 ± 40 nm for 110 µl / min and 469 ± 114 nm for 90 µl / min at a fixed gas pressure of 70 kPa. Thus, increasing the flow rate at a constant pressure reduces the nanoparticle size. When micrographs were closely examined, agglomeration between nanoparticles was observed. To prevent this, 0.5wt.% SA was added to 0.5wt.% PVA [56]. From the optical microscope images in Figure 3A, the size of 0.5 wt. % PVA-0.5 wt. % SA bubbles decreased from 323 ± 30 µm for 90 µl / min to 290 ± 31 µm for 110 µl / min at a constant gas pressure of 120 kPa. A similar situation was observed in the size of 0.5 wt. % PVA-0.5 wt. % SA nanoparticles. According images in Figure

3B, particle sizes decreased from 572 ± 86 nm for 90 µl / min to 386 ± 86 nm for 110 µl / min at a gas pressure of 120 kPa. SA added to 0.5 wt. % PVA solution increased the particle size. Considering that SA increases the particle size in all the PVA images, it was not added to PVA in the continuation of this research. The particle size was increased by the addition of SA to the pure PVA and the particle distribution was made more polydisperse. This may be due to the higher molecular weight of SA. In addition to that, agglomeration was prevented by adding SA as shown in figures 3A and 3B. Based on these results, it can be reported that addition of SA increased the size of the nanoparticles although it prevented agglomeration. One of the most crucial aims of this study was to produce the smallest nanoparticles, hence the PVA ratio was reduced from 0.5wt.% to 0.3wt.% because particle size increases when the PVA ratio was increased. In a study of Hüsler et al. [57], the average particle size was found to be 76 ± 2 µm with 2 wt.% PVA.

For the production of microbubbles containing 0.3wt.% PVA, the gas pressure was kept fixed at 40 kPa and the flow rates were raised from 40 to 80, 100, then 110 µl / min. When examining the optical microscope images of the bubbles (Figure 4), the rise in fluid flow rate caused a decrease in the diameter of the bubbles from 116 ± 5 µm to 101 ± 11 µm. Moreover, it was observed that the bubbles were distributed more regularly and monodisperse[37]. The SEM images of nanoparticles produced from these microbubbles demonstrated that the average diameters of the nanoparticles with different flow rates were 198 ± 35 nm for 40 µl / min, 141 ± 20 nm for 80 µl / min, 116 ± 13 nm for 100 µl / min, 70 ± 5 nm for 110 µl / min as shown in Figure 5. According to these results, it was clearly seen that the nanoparticles produced at the higher flow rate were more uniform[58]. In addition, the nanoparticles generated at the highest flow rate were of a constant size (~70 nm diameter).

It was observed that the process was optimized with 0.3 wt.% polyvinyl alcohol (PVA) solution, 40 kPa pressure, and 110 µl /min flow rate. The diameters of the bubbles and particles were

100 ± 10 μm and 70 ± 5 nm, respectively. Metformin was successfully loaded into nanoparticles in these optimized concentrations and parameters. The diameters of metformin-loaded bubbles and nanoparticles produced at the same flow rate and pressure are 102 ± 9 μm and 78 ± 5 nm, respectively (Figure 6). These results show that the addition of metformin to the PVA solution slightly affected the diameter of the bubbles and particles. In Figure 6, when the optical and SEM images of metformin-loaded PVA microbubbles and nanoparticles were examined, no drug crystals and clumps were observed on the surface. This proves that the drug was well-dispersed as supported by the literature [20,59,60].

The results of the FTIR analysis for PVA nanoparticles, metformin, and metformin-loaded PVA nanoparticles are shown in Figure 7. All major peaks clearly demonstrate the FTIR spectrum of PVA naonoparticles are indicated in Figure 7 (a). For example, the broadband observed between 3550 and 3200 cm^{-1} is associated with O-H stretching from strong intermolecular and intramolecular hydrogen bonds. Furthermore, the vibration band at 3000–2800 cm^{-1} is related to C-H of the alkyl groups. Peak at 1166 cm^{-1} indicates CO stretching[61,62]. Figure 7 (b) shows characteristic infrared bands of metformin, N-H stretching of the primary amine group at 3147 cm^{-1}, stretching and N-H bending vibrations of the primary amine group at 1574 cm^{-1}. The N-H bending / C-N stretching / C=O stretching band is at 1621 cm^{-1}. In addition, CH_3 asymmetric bending at 1472 cm^{-1}, C-H bending at 1445 cm^{-1}, CH_3 symmetrical bending vibration at 1417 cm^{-1}, and C=O tension at 1166 cm^{-1} were observed[63,64]. In Figure 7 (c), major peaks of metformin and PVA were obtained in the spectrum for nanoparticles loaded with metformin. Thus, successful drug encapsulation was achieved.

In vitro drug release studies were carried out with metformin-loaded 0.3wt.% PVA nanoparticles, optimised as described above. Firstly, the UV absorbance spectra obtained with the concentration range of metformin set from 4 to 14 μg/mL are shown in figure 8a. A linear standard calibration curve was constructed from the absorbance at 233 nm of metformin (R^2

=0.99) to calculate quantitative drug release data (Figure 8b). The encapsulation efficiency of drug-loaded nanopaticles is 78% according to eq.1. In vitro metformin release from nanoparticles was investigated in gastric (1.2 pH) and intestine (7.4 pH) fluids conditions at 37 ºC. As illustrated in figure 8c, the release of metformin in neutral condition is more gradual than in acidic. In gastric pH almost 42% of the drug was released during the first 10 minutes, while the corresponding figure for pH 7.4 was almost 30%. Metformin continued to be released at pH 7.4 for 240 minutes, whereas within 60 minutes at pH 1.2 the release amount reached almost 100%. This difference may be attributed to the fact that metformin was bi-protonated at this pH and this may cause unstable binding with PVA particles. These results are consistent with studies in which metformin has been produced for controlled release drug delivery systems [65].

Various kinetic release models were used to determine the release mechanism of metformin from PVA nanoparticles (obtained from the microbubbles) under neutral and acidic pH. The kinetic constants and regression coefficients (R^2) obtained from all samples after the zero order, first order, Higuchi, and tanh function models were fitted are given in Table 2. The tanh function had better agreement with higher R^2 values for both drug release profiles than other kinetics, which is consistent with Fickian diffusion, with a diffusion coefficient of about 10^{-19} m^2 s^{-1} for metformin in the polymer.

Conclusions

In the present study, different biopolymers such as PVA and SA were used and also metformin was loaded into optimized polymer concentration using a T-junction microfluidic device to produce microbubbles. Subsequently, homogeneous polymeric nanoparticles were obtained by bursting microbubbles. It has been shown that these nanoparticles can be used as nanocarriers for a hydrophilic drug such as metformin. Microbubbles/nanoparticles were optimized at 0.3 wt.% PVA solution, 40 kPa pressure, and 110 µl /min flow rate. The diameters of the bubbles

and particles were 100 ± 10 μm and 70 ± 5 nm, respectively. Metformin was successfully loaded into nanoparticles in these optimized concentrations and parameters. The nanoparticles had a smooth and uniform structure, and no drug crystals and clusters were seen on the surface. Metformin was released in a controlled manner at pH 1.2 for 60 min and at pH 7.4 for 240 min, and analysis suggests that release was by a simple Fickian diffusion process. Thus, metformin-loaded PVA nanoparticles produced with bursting microbubbles generated by using a T-junction device offer great potential in the treatment of T2DM, primarily because of their ability to metformin release in a controlled manner.

References

(1) Cam, M. E.; Hazar-Yavuz, A. N.; Yildiz, S.; Ertas, B.; Ayaz Adakul, B.; Taskin, T.; Alan, S.; Kabasakal, L. The Methanolic Extract of Thymus Praecox Subsp. Skorpilii Var. Skorpilii Restores Glucose Homeostasis, Ameliorates Insulin Resistance and Improves Pancreatic β-Cell Function on Streptozotocin/Nicotinamide-Induced Type 2 Diabetic Rats. *J. Ethnopharmacol*. **2019,** *231,* **29-38.** https://doi.org/10.1016/j.jep.2018.10.028.

(2) Çam, M. E.; Yildiz, S.; Ertaş, B.; Acar, A. E.; Taşkin, T.; Kabasakal, L. Antidiabetic Effects of Salvia Triloba and Thymus Praecox Subsp. Skorpilii Var. Skorpilii in a Rat Model of Streptozotocin/Nicotinamide-Induced Diabetes. *Marmara Pharm. J*. **2017**, *21*(4), 818-827. https://doi.org/10.12991/mpj.2017.8.

(3) Ilhan, E.; Cesur, S.; Guler, E.; Topal, F.; Albayrak, D.; Guncu, M. M.; Cam, M. E.; Taskin, T.; Sasmazel, H. T.; Aksu, B.; Oktar, F. N.; Gunduz, O. Development of Satureja Cuneifolia-Loaded Sodium Alginate/Polyethylene Glycol Scaffolds Produced by 3D-Printing Technology as a Diabetic Wound Dressing Material. *Int. J. Biol. Macromol*. **2020**, *161*, 1040-1054. https://doi.org/10.1016/j.ijbiomac.2020.06.086.

(4) Chaudhury, A.; Duvoor, C.; Reddy Dendi, V. S.; Kraleti, S.; Chada, A.; Ravilla, R.; Marco, A.; Shekhawat, N. S.; Montales, M. T.; Kuriakose, K.; Sasapu, A.; Beebe, A.; Patil, N.; Musham, C. K.; Lohani, G. P.; Mirza, W. Clinical Review of Antidiabetic Drugs: Implications for Type 2 Diabetes Mellitus Management. *Frontiers in Endocrinology*. **2017**, *8*(6), 1-12. https://doi.org/10.3389/fendo.2017.0006.

(5) Jia, Y.; Lao, Y.; Zhu, H.; Li, N.; Leung, S. W. Is Metformin Still the Most Efficacious First-Line Oral Hypoglycaemic Drug in Treating Type 2 Diabetes? A Network Meta-Analysis of Randomized Controlled Trials. *Obesity Reviews*. **2019**, *20*(1), 1-12.

https://doi.org/10.1111/obr.12753.

(6) Cam, M. E.; Crabbe-Mann, M.; Alenezi, H.; Hazar-Yavuz, A. N.; Ertas, B.; Ekentok, C.; Ozcan, G. S.; Topal, F.; Guler, E.; Yazir, Y.; Parhizkar, M.; Edirisinghe, M. The Comparision of Glybenclamide and Metformin-Loaded Bacterial Cellulose/Gelatin Nanofibres Produced by a Portable Electrohydrodynamic Gun for Diabetic Wound Healing. *Eur*. *Polym*. *J*. **2020,** *134*, 109844. https://doi.org/10.1016/j.eurpolymj.2020.109844.

(7) Kanto, K.; Ito, H.; Noso, S.; Babaya, N.; Hiromine, Y.; Taketomo, Y.; Toma, J.; Niwano, F.; Yasutake, S.; Kawabata, Y.; Ikegami, H. Effects of Dosage and Dosing Frequency on the Efficacy and Safety of High-Dose Metformin in Japanese Patients with Type 2 Diabetes Mellitus. *J*. *Diabetes Investig*. **2018,** *9*(3), 587-593. https://doi.org/10.1111/jdi.12755.

(8) Nasri, H.; Rafieian-Kopaei, M. Metformin: Current Knowledge. *Journal of Research in Medical Sciences*. **2014**, *19*(7), 658.

(9) Kang, S. T.; Yeh, C. K. Ultrasound Microbubble Contrast Agents for Diagnostic and Therapeutic Applications: Current Status and Future Design. *Chang Gung Medical Journal*. **2012**, *35*(2), 125-139. https://doi.org/10.4103/2319-4170.106159.

(10) Unger, E. C.; Hersh, E.; Vannan, M.; Matsunaga, T. O.; McCreery, T. Local Drug and Gene Delivery through Microbubbles. *Prog*. *Cardiovasc*. *Dis*. **2001**, *44*, 45-54. https://doi.org/10.1053/pcad.2001.26443.

(11) Campbell, G. M.; Mougeot, E. Creation and Characterisation of Aerated Food Products. *Trends Food Sci*. *Technol*. **1999**, *10*(9), 283-296.https://doi.org/10.1016/S0924-2244(00)00008-X.

(12) Anselmo, A. C.; Mitragotri, S. A Review of Clinical Translation of Inorganic Nanoparticles. *AAPS J*. **2015**, *17*(5), 1041-1054https://doi.org/10.1208/s12248-015-9780-2.

(13) Lee Chung, B.; Toth, M. J.; Kamaly, N.; Sei, Y. J.; Becraft, J.; Mulder, W. J. M.; Fayad, Z. A.; Farokhzad, O. C.; Kim, Y. T.; Langer, R. Nanomedicines for Endothelial Disorders. *Nano Today*. **2015**, *10*(6), 759-776. https://doi.org/10.1016/j.nantod.2015.11.009.

(14) Galmarini, S.; Hanusch, U.; Giraud, M.; Cayla, N.; Chiappe, D.; Von Moos, N.; Hofmann, H.; Maurizi, L. Beyond Unpredictability: The Importance of Reproducibility in Understanding the Protein Corona of Nanoparticles. *Bioconjug*. *Chem*. **2018**, *29*(10), 3385-3393. https://doi.org/10.1021/acs.bioconjchem.8b00554.

(15) Chan, E. M.; Alivisatos, A. P.; Mathies, R. A. High-Temperature Microfluidic Synthesis of CdSe Nanocrystals in Nanoliter Droplets. *J*. *Am*. *Chem*. *Soc*. **2005**. *127*(40), 13854- 13861. https://doi.org/10.1021/ja051381p.

(16) Chang, M. W.; Stride, E.; Edirisinghe, M. A New Method for the Preparation of Monoporous Hollow Microspheres. *Langmuir* **2010**, *26*(7), 5115-5121. https://doi.org/10.1021/la903592s.

(17) Nie, Z.; Li, W.; Seo, M.; Xu, S.; Kumacheva, E. Janus and Ternary Particles Generated by Microfluidic Synthesis: Design, Synthesis, and Self-Assembly. *J*. *Am*. *Chem*. *Soc*. **2006**, *128*(29), 9408-9412. https://doi.org/10.1021/ja060882n.

(18) Cui, W.; Lu, X.; Cui, K.; Wu, J.; Wei, Y.; Lu, Q. Photosensitive Nanoparticles of Chitosan Complex for Controlled Release of Dye Molecules. *Nanotechnology* **2011**, *22*(6), 065702. https://doi.org/10.1088/0957-4484/22/6/065702.

(19) Chinnaiyan, S. K.; Karthikeyan, D.; Gadela, V. R. Development and Characterization of Metformin Loaded Pectin Nanoparticles for T2 Diabetes Mellitus. *Pharm*. *Nanotechnol*. **2018**, *6*(4), 253-263. https://doi.org/10.2174/2211738507666181221142406.

(20) Pereira, A. de S. B. F.; Brito, G. A. de C.; Lima, M. L. de S.; Silva Júnior, A. A. da; Silva, E. D. S.; de Rezende, A. A.; Bortolin, R. H.; Galvan, M.; Pirih, F. Q.; Araújo Júnior, R. F. de; Medeiros, C. A. C. X. de; Guerra, G. C. B.; Araújo, A. A. de. Metformin Hydrochloride-Loaded PLGA Nanoparticle in Periodontal Disease Experimental Model Using Diabetic Rats. *Int*. *J*. *Mol*. *Sci*. **2018**, *19*(11), 3488. https://doi.org/10.3390/ijms19113488.

(21) Kumar, S.; Bhanjana, G.; Verma, R. K.; Dhingra, D.; Dilbaghi, N.; Kim, K. H. Metformin-Loaded Alginate Nanoparticles as an Effective Antidiabetic Agent for Controlled Drug Release. *J*. *Pharm*. *Pharmacol*. **2017**, *69(*2), 143- 150. https://doi.org/10.1111/jphp.12672.

(22) Mokhtare, B.; Ozakar, R. S.; Bayrakceken, H. Preparation of Metformin HCl-Loaded Chitosan Microspheres and In Vitro Characterization Studies. **2015**, *35* (1), 74–86.

(23) Aldea, M.; Florian, I. S.; Potara, M.; Soritau, O.; Nagy-Simon, T.; Kacso, G. Metformin Delivery Using Chitosan-Capped Gold Nanoparticles in Glioblastoma Cell Lines. *Rom*. *Neurosurg*. **2018**, *32* (2), 230–239. https://doi.org/10.2478/romneu-2018-0030.

(24) Xu, Q.; Zhu, T.; Yi, C.; Shen, Q. Characterization and Evaluation of Metformin-Loaded Solid Lipid Nanoparticles for Celluar and Mitochondrial Uptake. *Drug Dev*. *Ind*. *Pharm*. **2016**, *42*(5), 701-706. https://doi.org/10.3109/03639045.2015.1075028.

(25) Ashok Kumar, A.; Balakrishna, T.; Jash, R.; Murthy, T. E. G. K.; Anil Kumar, A.;

Sudheer, B. Formulation and Evaluation of Mucoadhesive Microcapsules of Metformin HCl with Gum Karaya. *Int*. *J*. *Pharm*. *Pharm*. *Sci*. **2011**, *3* (3), 150–155.

(26) Cao, J.; Liu, H.; Pan, W.; Sun, C.; Feng, Y.; Zhong, H.; Shi, S. S.; He, Y. The Preparation of the Sustained Release Metformin Hydrochloride Microcapsules by the Wurster Fluidized Bed. *Pak*. *J*. *Pharm*. *Sci*. **2014**, 27, 779–784.

(27) Cetin, M.; Atila, A.; Sahin, S.; Vural, I. Preparation and Characterization of Metformin Hydrochloride Loaded-Eudragit®RSPO and Eudragit®RSPO/PLGA Nanoparticles. *Pharm*. *Dev*. *Technol*. **2013**, 18, 570–576. https://doi.org/10.3109/10837450.2011.604783.

(28) Gunduz, O.; Ahmad, Z.; Stride, E.; Edirisinghe, M. A Device for the Fabrication of Multifunctional Particles from Microbubble Suspensions. *Mater*. *Sci*. *Eng*. *C* **2012**, *32*(4), 1005-1010. https://doi.org/10.1016/j.msec.2012.01.018.

(29) Fallahi, H.; Zhang, J.; Nicholls, J.; Phan, H. P.; Nguyen, N. T. Stretchable Inertial Microfluidic Device for Tunable Particle Separation. *Anal*. *Chem*. **2020**, *92*(18), 12473-12480. https://doi.org/10.1021/acs.analchem.0c02294.

(30) Berlanda, S. F.; Breitfeld, M.; Dietsche, C. L.; Dittrich, P. S. Recent Advances in Microfluidic Technology for Bioanalysis and Diagnostics. *Analytical Chemistry*. **2021**, *93*, 1, 311–331. https://doi.org/10.1021/acs.analchem.0c04366.

(31) McEwan, C.; Kamila, S.; Owen, J.; Nesbitt, H.; Callan, B.; Borden, M.; Nomikou, N.; Hamoudi, R. A.; Taylor, M. A.; Stride, E.; McHale, A. P.; Callan, J. F. Combined Sonodynamic and Antimetabolite Therapy for the Improved Treatment of Pancreatic Cancer Using Oxygen Loaded Microbubbles as a Delivery Vehicle. *Biomaterials* **2016**, *80*, 20-32. https://doi.org/10.1016/j.biomaterials.2015.11.033.

(32) Kucuk, I. Polymer Nanospheres Formed by a Microfluidic Technique with Evans Blue Dye. *Polym*. *Adv*. *Technol*. **2017**, *28* (8), 940–946. https://doi.org/10.1002/pat.3641.

(33) Stride, E.; Pancholi, K.; Edirisinghe, M. J.; Samarasinghe, S. Increasing the Nonlinear Character of Microbubble Oscillations at Low Acoustic Pressures. *J*. *R*. *Soc*. *Interface* **2008**, *5*(24), 807-811.https://doi.org/10.1098/rsif.2008.0005.

(34) Seo, M.; Nie, Z.; Xu, S.; Mok, M.; Lewis, P. C.; Graham, R.; Kumacheva, E. Continuous Microfluidic Reactors for Polymer Particles. *Langmuir* **2005**, *21*(25), 11614-11622. https://doi.org/10.1021/la050519e.

(35) Wang, R. Nanoparticles Influence Droplet Formation in a T-Shaped Microfluidic. *J*. *Nanoparticle Res*. **2013**, *15*(12), 1-9. https://doi.org/10.1007/s11051-013-2128-x.

(36) Xu, J. H.; Dong, P. F.; Zhao, H.; Tostado, C. P.; Luo, G. S. The Dynamic Effects of Surfactants on Droplet Formation in Coaxial Microfluidic Devices. *Langmuir* **2012**, *28*(25), 9250-9258. https://doi.org/10.1021/la301363d.

(37) Parhizkar, M.; Edirisinghe, M.; Stride, E. Effect of Operating Conditions and Liquid Physical Properties on the Size of Monodisperse Microbubbles Produced in a Capillary Embedded T-Junction Device. *Microfluid*. *Nanofluidics* **2013**, *14* (5), 797–808. https://doi.org/10.1007/s10404-012-1098-0.

(38) Alenezi, H.; Cam, M. E.; Edirisinghe, M. Experimental and Theoretical Investigation of the Fluid Behavior during Polymeric Fiber Formation with and without Pressure. *Appl*. *Phys*. *Rev*. **2019**. *6*(4), 041401. https://doi.org/10.1063/1.5110965.

(39) Liu, X.; Holzwarth, J. M.; Ma, P. X. Functionalized Synthetic Biodegradable Polymer Scaffolds for Tissue Engineering. *Macromolecular Bioscience*. **2012,** *12(*7), 911- 919. https://doi.org/10.1002/mabi.201100466.

(40) Gomes, M. E.; Reis, R. L. Biodegradable Polymers and Composites in Biomedical Applications: From Catgut to Tissue Engineering Part 1 Available Systems and Their Properties. *International Materials Reviews*. **2004**, *49*(5), 261-273. https://doi.org/10.1179/095066004225021918.

(41) Jiang, S.; Liu, S.; Feng, W. PVA Hydrogel Properties for Biomedical Application. *J*. *Mech*. *Behav*. *Biomed*. *Mater*. **2011**, *4*(7), 1228-1233. https://doi.org/10.1016/j.jmbbm.2011.04.005.

(42) Cesur, S.; Cam, M. E.; Sayın, F. S.; Su, S.; Gunduz, O. Controlled Release of Metformin Loaded Polyvinyl Alcohol (PVA) Microbubble/Nanoparticles Using Microfluidic Device for the Treatment of Type 2 Diabetes Mellitus. In *Lecture Notes in Computer Science (including subseries Lecture Notes in Artificial Intelligence and Lecture Notes in Bioinformatics)*; **2020**, 185-193. https://doi.org/10.1007/978-3-030-45385-5_17.

(43) Paradossi, G.; Cavalieri, F.; Chiessi, E.; Spagnoli, C.; Cowman, M. K. Poly(Vinyl Alcohol) as Versatile Biomaterial for Potential Biomedical Applications. In *Journal of Materials Science: Materials in Medicine*; **2003**, *14*(8), 687-691. https://doi.org/10.1023/A:1024907615244.

(44) Ali, I. O. Synthesis and Characterization of Ag0/PVA Nanoparticles via Photo- and Chemical Reduction Methods for Antibacterial Study. *Colloids Surfaces A Physicochem*. *Eng*. *Asp*. **2013**, 436, 922-929. https://doi.org/10.1016/j.colsurfa.2013.08.032.

(45) Limpan, N.; Prodpran, T.; Benjakul, S.; Prasarpran, S. Influences of Degree of Hydrolysis and Molecular Weight of Poly(Vinyl Alcohol) (PVA) on Properties of Fish Myofibrillar Protein/PVA Blend Films. *Food Hydrocoll*. **2012**, *29(*1), 226-233.

https://doi.org/10.1016/j.foodhyd.2012.03.007.

(46) Aranci, K.; Uzun, M.; Su, S.; Cesur, S.; Ulag, S.; Amin, A.; Guncu, M. M.; Aksu, B.; Kolayli, S.; Ustundag, C. B.; Silva, J. C.; Ficai, D.; Ficai, A.; Gunduz, O. 3D Propolis-Sodium Alginate Scaffolds: Influence on Structural Parameters, Release Mechanisms, Cell Cytotoxicity and Antibacterial Activity. *Molecules* **2020**, *25*(21), 5082. https://doi.org/10.3390/molecules25215082.

(47) Gombotz, W. R.; Wee, S. F. Protein Release from Alginate Matrices. *Advanced Drug Delivery Reviews*. **2012,** *31*(3), 267-285. https://doi.org/10.1016/j.addr.2012.09.007.

(48) Wu, J.; Wei, W.; Wang, L. Y.; Su, Z. G.; Ma, G. H. A Thermosensitive Hydrogel Based on Quaternized Chitosan and Poly(Ethylene Glycol) for Nasal Drug Delivery System. *Biomaterials* **2007**, *28*(13), 2220-2232. https://doi.org/10.1016/j.biomaterials.2006.12.024.

(49) Elsayed, M.; Huang, J.; Edirisinghe, M. Bioinspired Preparation of Alginate Nanoparticles Using Microbubble Bursting. *Mater*. *Sci*. *Eng*. *C* **2015**, *46*, 132–139. https://doi.org/10.1016/j.msec.2014.09.036.

(50) Gunduz, O.; Ahmad, Z.; Stride, E.; Tamerler, C.; Edirisinghe, M. Bioinspired Bubble Design for Particle Generation. *J*. *R*. *Soc*. *Interface* **2012**, *9*(67), 389-395. https://doi.org/10.1098/rsif.2011.0671.

(51) Gunduz, O.; Ahmad, Z.; Stride, E.; Edirisinghe, M. Continuous Generation of Ethyl Cellulose Drug Delivery Nanocarriers from Microbubbles. *Pharm*. *Res*. **2013**, *30*(1), 225-237.https://doi.org/10.1007/s11095-012-0865-7.

(52) Parhizkar, M.; Edirisinghe, M.; Stride, E. The Effect of Surfactant Type and Concentration on the Size and Stability of Microbubbles Produced in a Capillary

Embedded T-Junction Device. *RSC Adv*. **2015**, *5* (14), 10751–10762. https://doi.org/10.1039/c4ra15167d.

(53) Božič, M.; Elschner, T.; Tkaučič, D.; Bračič, M.; Hribernik, S.; Stana Kleinschek, K.; Kargl, R. Effect of Different Surface Active Polysaccharide Derivatives on the Formation of Ethyl Cellulose Particles by the Emulsion-Solvent Evaporation Method. *Cellulose* **2018**. *25*(12), 6901-6922. https://doi.org/10.1007/s10570-018-2062-2.

(54) Cesur, S.; Oktar, F. N.; Ekren, N.; Kilic, O.; Alkaya, D. B.; Seyhan, S. A.; Ege, Z. R.; Lin, C.-C.; Kuruca, S. E.; Erdemir, G.; Gunduz, O. Preparation and Characterization of Electrospun Polylactic Acid/Sodium Alginate/Orange Oyster Shell Composite Nanofiber for Biomedical Application. *J*. *Aust*. *Ceram*. *Soc*. **2019**, 1-11. https://doi.org/10.1007/s41779-019-00363-1.

(55) Kucuk, I.; Yilmaz, N. F.; Sinan, A. Effects of Junction Angle and Gas Pressure on Polymer Nanosphere Preparation from Microbubbles Bursted in a Combined Microfluidic Device with Thin Capillaries. *J*. *Mol*. *Struct*. **2018**, 1173, 422-427. https://doi.org/10.1016/j.molstruc.2018.06.084.

(56) Pham, D. Van; Tho Bach, L. Immobilized Bacteria by Using PVA (Polyvinyl Alcohol) Crosslinked with Sodium Sulfate. *Int*. *J*. *Sci*. *Eng*. **2014**, *7*(1), 41-47. https://doi.org/10.12777/ijse.7.1.41-47.

(57) Hüsler, A.; Haas, S.; Parry, L.; Romero, M.; Nisisako, T.; Williams, P.; Wildman, R. D.; Alexander, M. R. Effect of Surfactant on: Pseudomonas Aeruginosa Colonization of Polymer Microparticles and Flat Films. *RSC Adv*. **2018**, *8*(28), 15352-15357. https://doi.org/10.1039/c8ra01491d.

(58) Amoyav, B.; Benny, O. Controlled and Tunable Polymer Particles' Production Using a Single Microfluidic Device. *Appl*. *Nanosci*. **2018**, *8*(4), 905-914.

https://doi.org/10.1007/s13204-018-0790-0.

(59) Ngawhirunpat, T.; Opanasopit, P.; Rojanarata, T.; Akkaramongkolporn, P.; Ruktanonchai, U.; Supaphol, P. Development of Meloxicam-Loaded Electrospun Polyvinyl Alcohol Mats as a Transdermal Therapeutic Agent. *Pharm*. *Dev*. *Technol*. **2009**, *14*(1), 73-82. https://doi.org/10.1080/10837450802409420.

(60) Zeng, J.; Yang, L.; Liang, Q.; Zhang, X.; Guan, H.; Xu, X.; Chen, X.; Jing, X. Influence of the Drug Compatibility with Polymer Solution on the Release Kinetics of Electrospun Fiber Formulation. *J*. *Control*. *Release* **2005**, *105*(1-2), 43-51.https://doi.org/10.1016/j.jconrel.2005.02.024.

(61) Alhosseini, S. N.; Moztarzadeh, F.; Mozafari, M.; Asgari, S.; Dodel, M.; Samadikuchaksaraei, A.; Kargozar, S.; Jalali, N. Synthesis and Characterization of Electrospun Polyvinyl Alcohol Nanofibrous Scaffolds Modified by Blending with Chitosan for Neural Tissue Engineering. *Int*. *J*. *Nanomedicine* **2012**, *7*, 25.

(62) Roberts, M. J.; Bentley, M. D.; Harris, J. M. Chemistry for Peptide and Protein PEGylation. *Adv*. *Drug Deliv*. *Rev*. **2012,** *64*, 116-127. https://doi.org/10.1016/j.addr.2012.09.025

(63) Kim, D. W.; Park, J. B. Development and Pharmaceutical Approach for Sustained-Released Metformin Succinate Tablets. *J*. *Drug Deliv*. *Sci*. *Technol*. **2015**, *30,* 90-99. https://doi.org/10.1016/j.jddst.2015.09.019.

(64) Nurani, M.; Akbari, V.; Taheri, A. Preparation and Characterization of Metformin Surface Modified Cellulose Nanofiber Gel and Evaluation of Its Anti-Metastatic Potentials. *Carbohydr*. *Polym*. **2017,** *165*, 322-333. https://doi.org/10.1016/j.carbpol.2017.02.067.

(65) Patiño-Herrera, R.; Louvier-Hernández, J. F.; Escamilla-Silva, E. M.; Chaumel, J.; Escobedo, A. G. P.; Pérez, E. Prolonged Release of Metformin by SiO 2 Nanoparticles Pellets for Type II Diabetes Control. *Eur*. *J*. *Pharm*. *Sci*. **2019**, *131*, 1-8. https://doi.org/10.1016/j.ejps.2019.02.003.

Captions for Figures and Tables

Table 1. Physical characterics of solutions used

Table 2. Results from four kinetic models of metformin release from metformin-loaded PVA nanoparticles at different pH values

Figure 1. Schematic drawing showing the process of obtaining microbubbles/nanoparticles using T-junction microfluidic device

Figure 2. A) Optical images of 0.5 wt.% PVA bubbles prepared at various flow rates (90 and 110 μl/min) and their size distributions. B) Scanning electron microscopy (SEM) images of 0.5 wt. % PVA nanoparticles prepared at various flow rates (90 and 110 μl/min) and their diameter distributions

Figure 4. A) Optical images of (0.5 wt. % PVA-0.5 wt. % SA) bubbles prepared at various flow rates (90 and 110 μl/min) and their size distributions. B) Scanning electron microscopy (SEM) images of (0.5 wt. % PVA-0.5 wt. % SA) nanoparticles prepared at various flow rates (90 and 110 μl/min) and their diameter distributions

Figure 6. Optical images of 0.3 wt. % PVA bubbles prepared at various flow rates (40, 80,100, and 110 µl/min) and their size distributions.

Figure 5. Scanning electron microscopy (SEM) images of 0.3 wt. % PVA nanoparticles prepared at various flow rate (40, 80, 100, and 110 µl/min) and their diameter distributions

Figure 6. Metformin-loaded microbubbles / nanoparticles prepared at 110 µl / min flow rate and 40 kPa. Optical microscope images and diameters of microbubbles (A), SEM images and diameter distributions of nanoparticles (B)

Figure 7. FTIR Spectra of a) PVA nanoparticles, b) metformin, and c) the resultant PVA/Metformin nanoparticles.

Figure 8. a) UV absorbance spectra of metformin and b) Calibration curve for metformin at 233 nm. c) In vitro release studies of metformin from nanoparticles under acidic (PBS, pH 1.2) and neutral (PBS, pH 7.4) environments. Each bar represents as average (n = 3) ± SD

Table 1

Concentration of Solutions	Density (kg/m^3)	Surface Tension (mN/m)	Viscosity (mPa s)
0.3 wt. % PVA	0.98	42. 9	286
0.5 wt. % PVA	0.99	42. 4	300
0.5 wt.% (PVA-SA)	1.00	44.9	330
0.3 wt. % PVA/0.2 wt. Metformin	0.99	43.0	290

Table 2

	Zero Order		**First Order**		**Higuchi**		**tanh**	
Sample	R^2	K_o	R^2	K_1	R^2	K_h	R^2	n
Ph 7.4	0.327	4.760	0.721	0.107	0.765	17.53	0.953	0.236
Ph 1.2	0.443	8.988	0.504	0.214	0.593	26.87	0.721	0.350

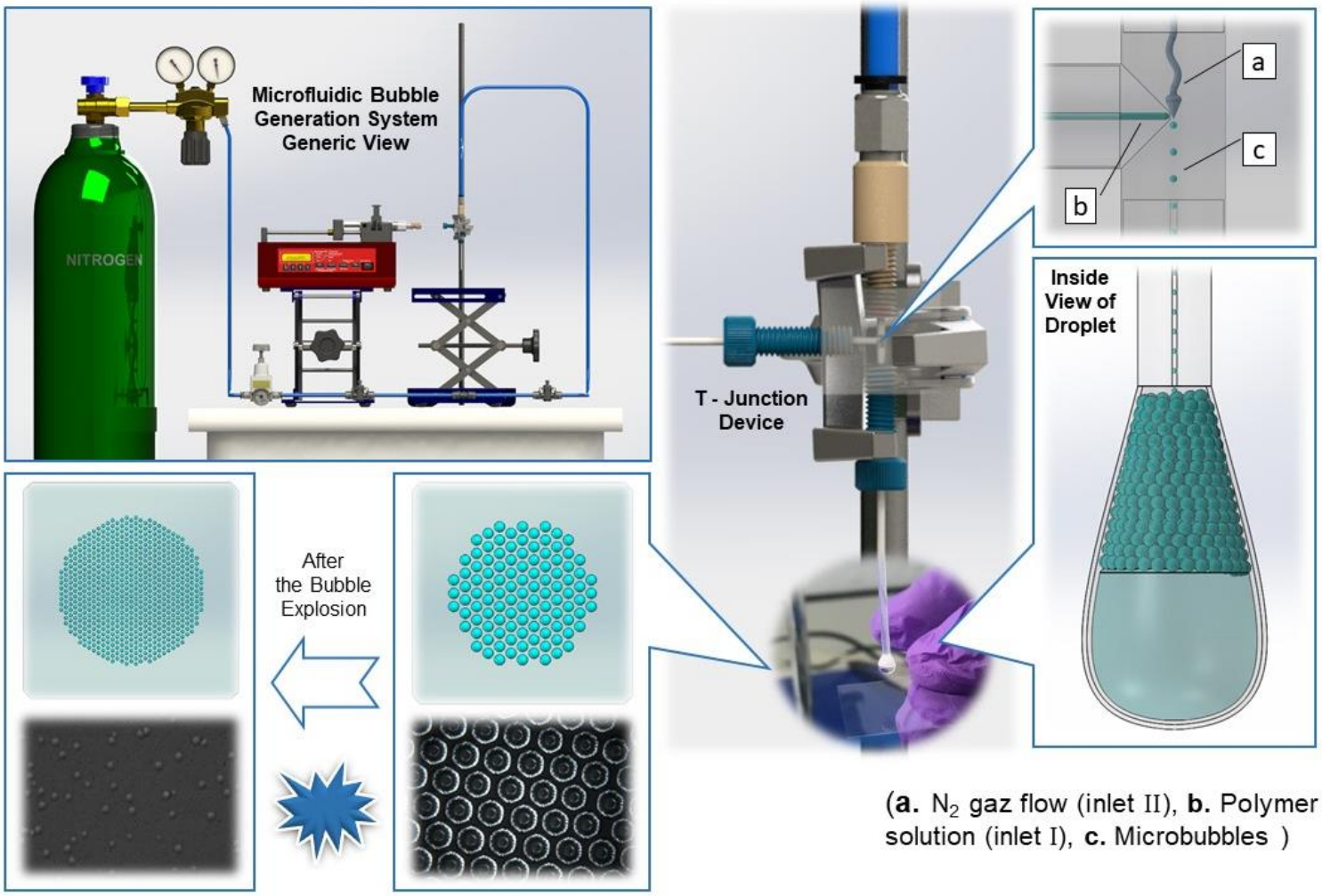
Microfluidic Bubble Generation System Generic View
NITROGEN
T - Junction Device
a
b
c
Inside View of Droplet
After the Bubble Explosion
(a. N_2 gaz flow (inlet II), b. Polymer solution (inlet I), c. Microbubbles)

Figure 1

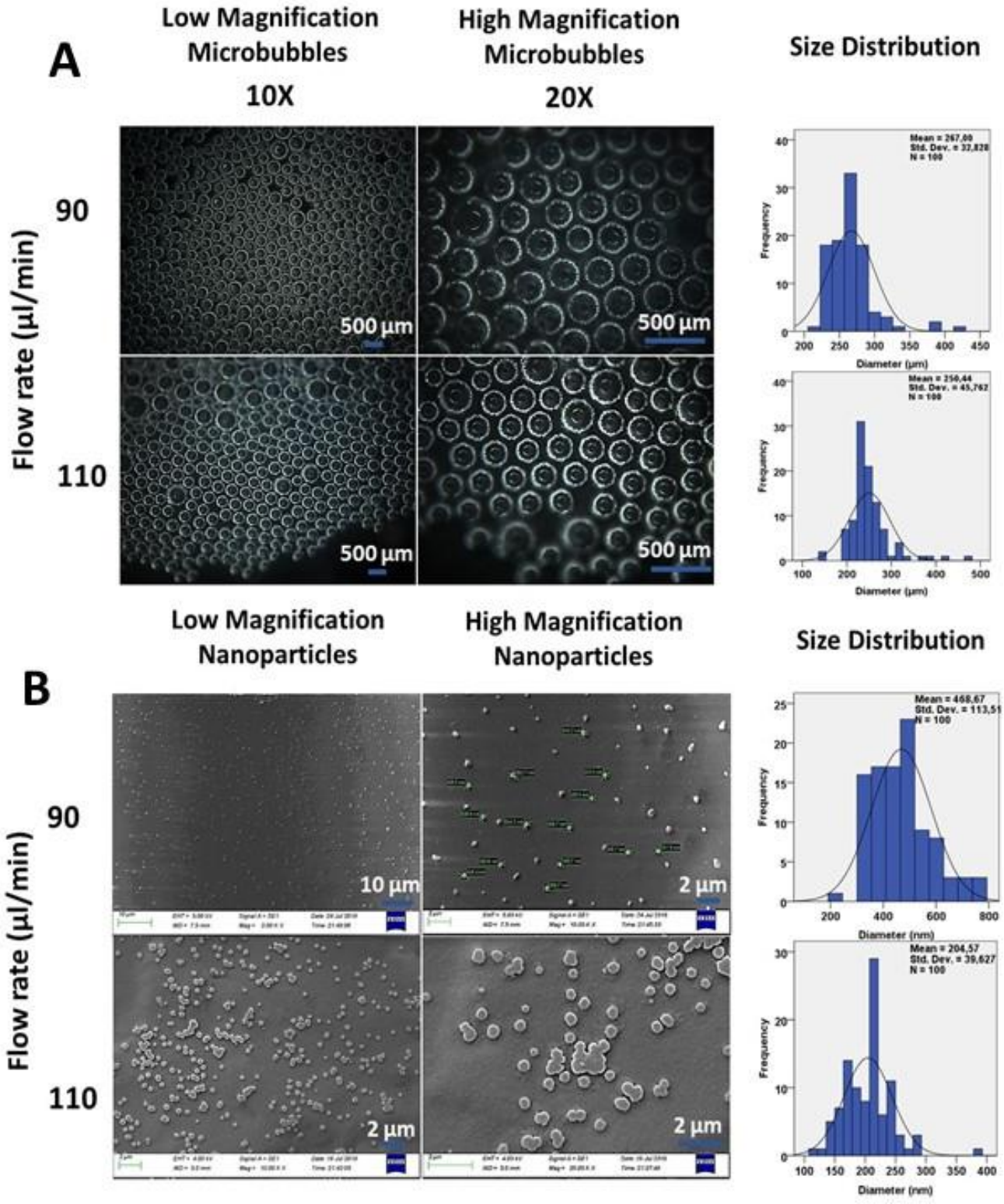
A
Low Magnification Microbubbles
10X
High Magnification Microbubbles
20X
Size Distribution
Flow rate (µl/min)
90
110
500 µm
500 µm
500 µm
500 µm
Mean = 267,00
Std. Dev. = 32,828
N = 100
Frequency
Diameter (µm)
Mean = 250,44
Std. Dev. = 45,762
N = 100
Frequency
Diameter (µm)
B
Low Magnification Nanoparticles
High Magnification Nanoparticles
Size Distribution
Flow rate (µl/min)
90
110
10 µm
2 µm
2 µm
2 µm
Mean = 468,67
Std. Dev. = 113,51
N = 100
Frequency
Diameter (nm)
Mean = 204,57
Std. Dev. = 39,627
N = 100
Frequency
Diameter (nm)

Figure 2

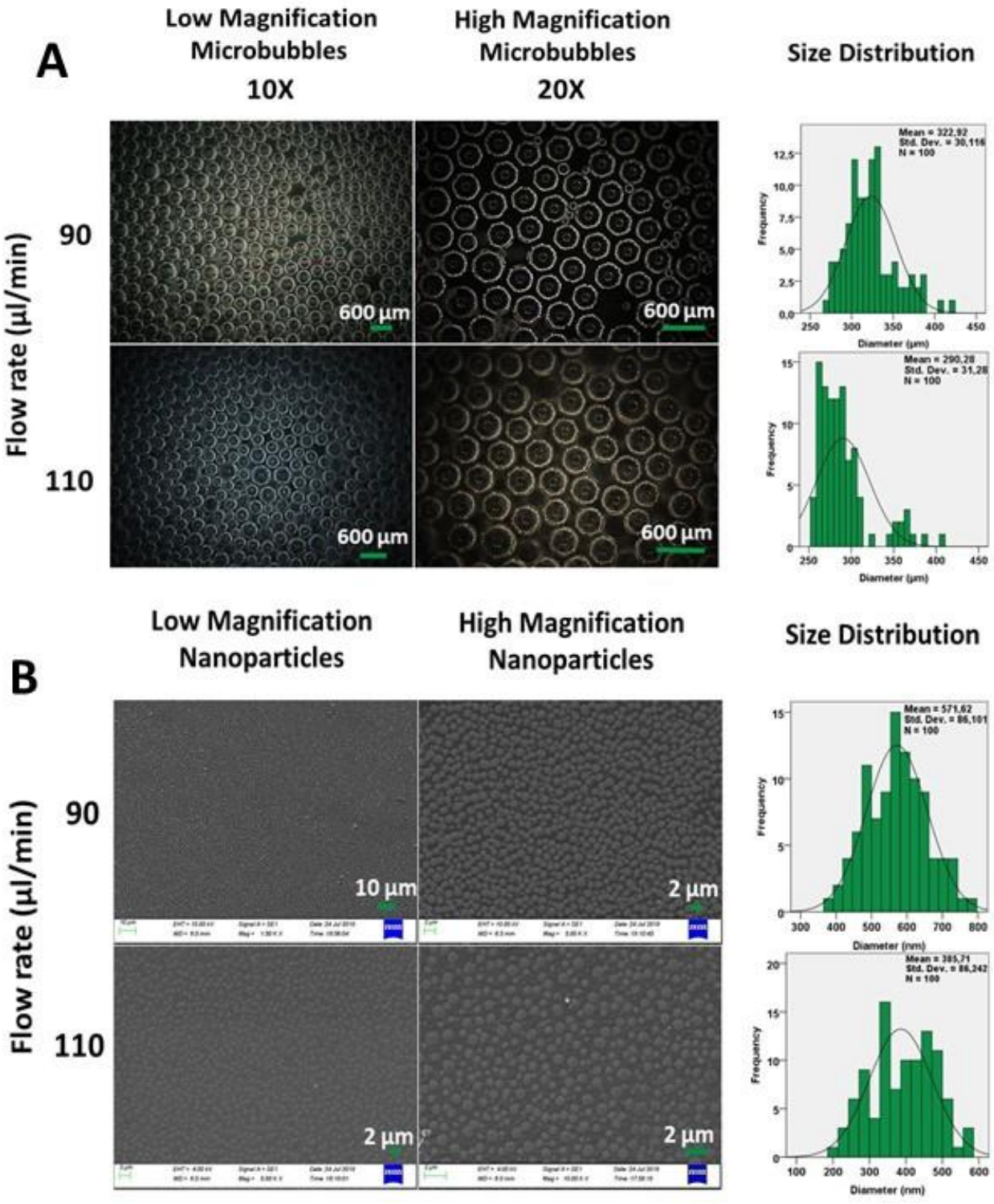
A
Low Magnification
Microbubbles
10X
High Magnification
Microbubbles
20X
Size Distribution
Flow rate (µl/min)
90
110
600 µm
600 µm
600 µm
600 µm
Mean = 322,92
Std. Dev. = 30,116
N = 100
Mean = 290,28
Std. Dev. = 31,28
N = 100
Frequency
Diameter (µm)
B
Low Magnification
Nanoparticles
High Magnification
Nanoparticles
Size Distribution
Flow rate (µl/min)
90
110
10 µm
2 µm
2 µm
2 µm
Mean = 571,62
Std. Dev. = 86,101
N = 100
Mean = 385,71
Std. Dev. = 86,242
N = 100
Frequency
Diameter (nm)

Figure 3

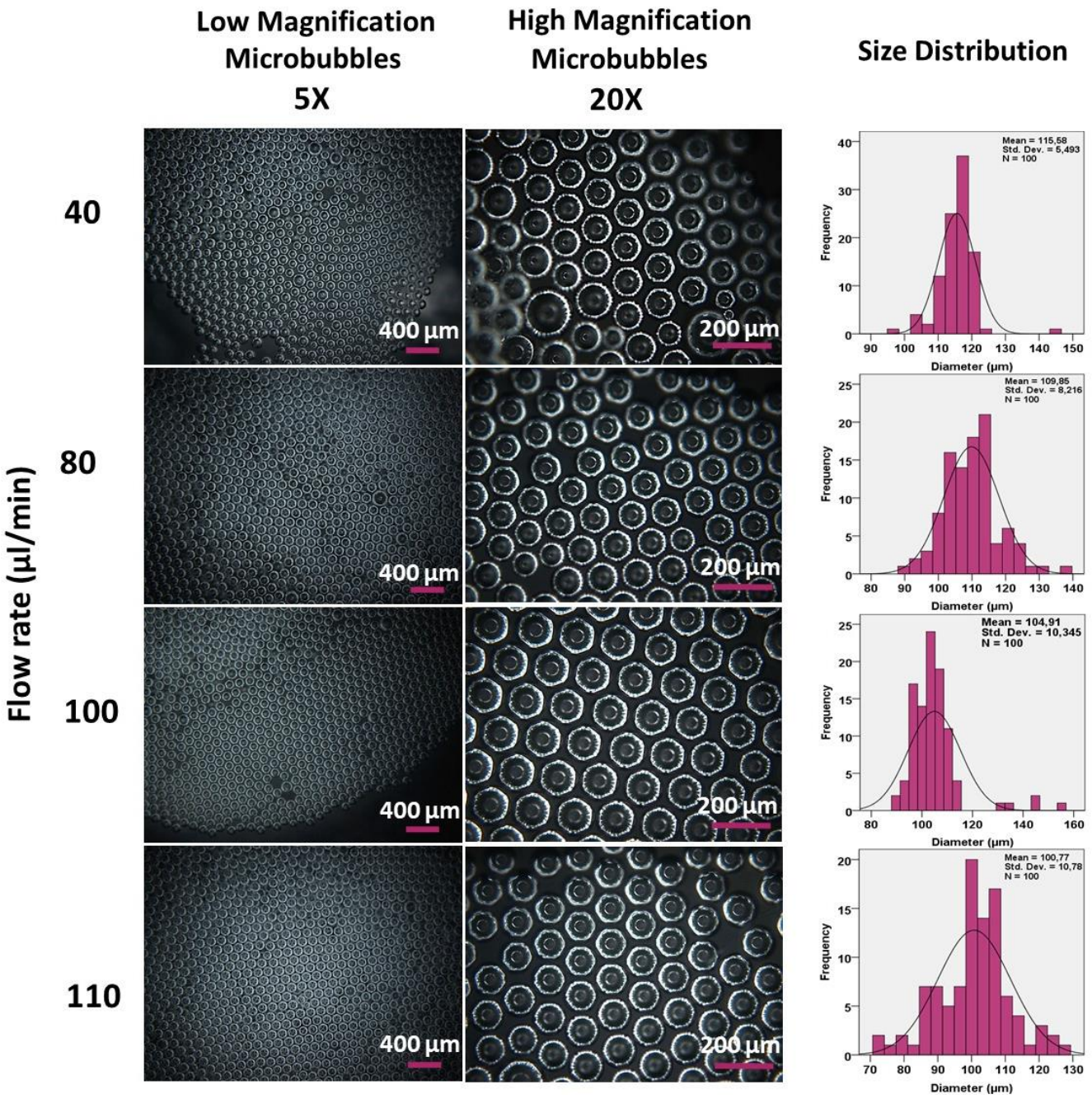
Low Magnification Microbubbles 5X
High Magnification Microbubbles 20X
Size Distribution
Flow rate (µl/min)
40
80
100
110
400 µm
200 µm
Mean = 115,58
Std. Dev. = 5,493
N = 100
Mean = 109,85
Std. Dev. = 8,216
N = 100
Mean = 104,91
Std. Dev. = 10,345
N = 100
Mean = 100,77
Std. Dev. = 10,78
N = 100
Frequency
Diameter (µm)

Figure 4

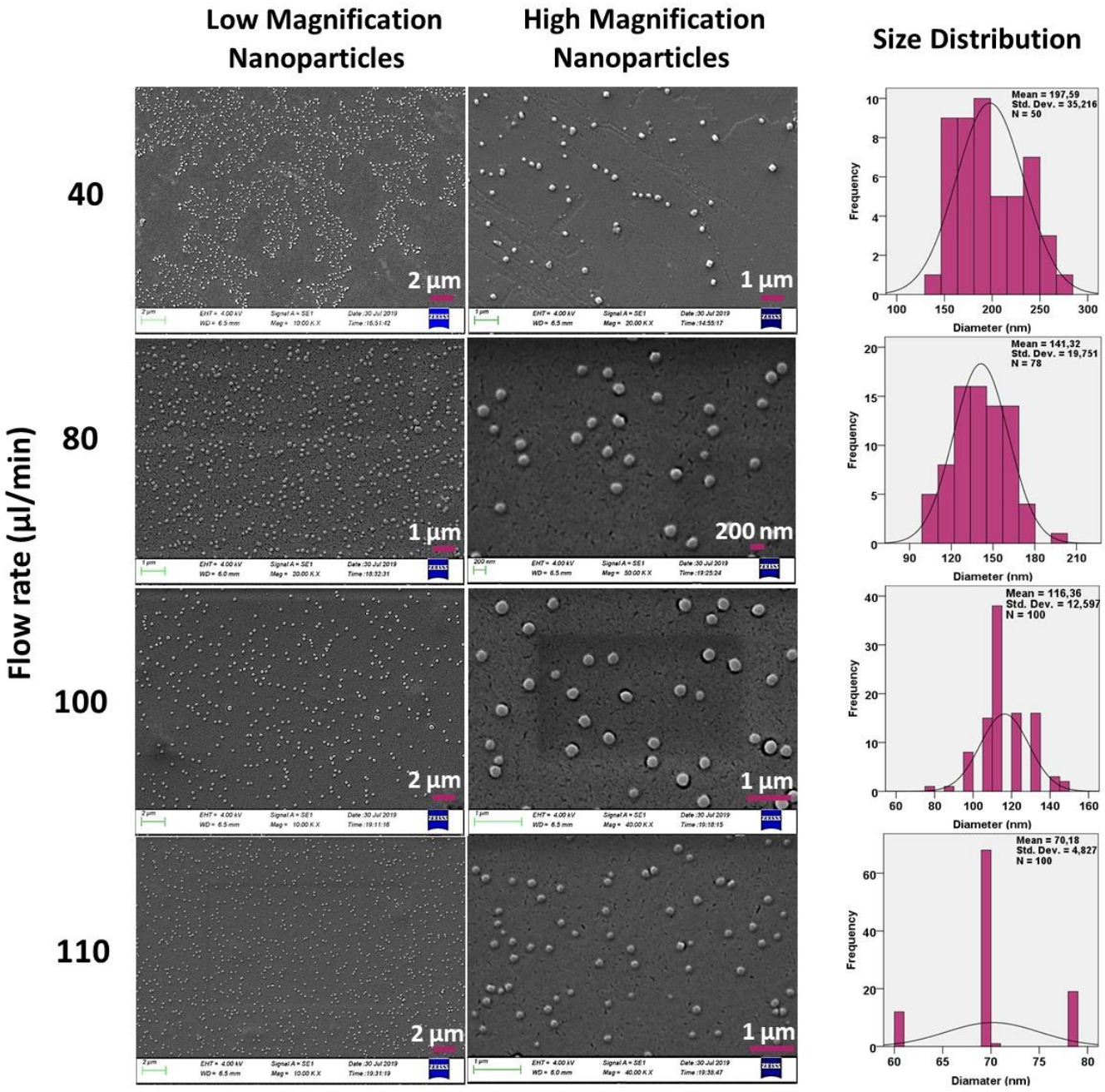
Low Magnification Nanoparticles
High Magnification Nanoparticles
Size Distribution
Flow rate (µl/min)
40
80
100
110
2 µm
1 µm
200 nm
Mean = 197,59
Std. Dev. = 35,216
N = 50
Mean = 141,32
Std. Dev. = 19,751
N = 78
Mean = 116,36
Std. Dev. = 12,597
N = 100
Mean = 70,18
Std. Dev. = 4,827
N = 100
Frequency
Diameter (nm)
Diamater (nm)

Figure 5

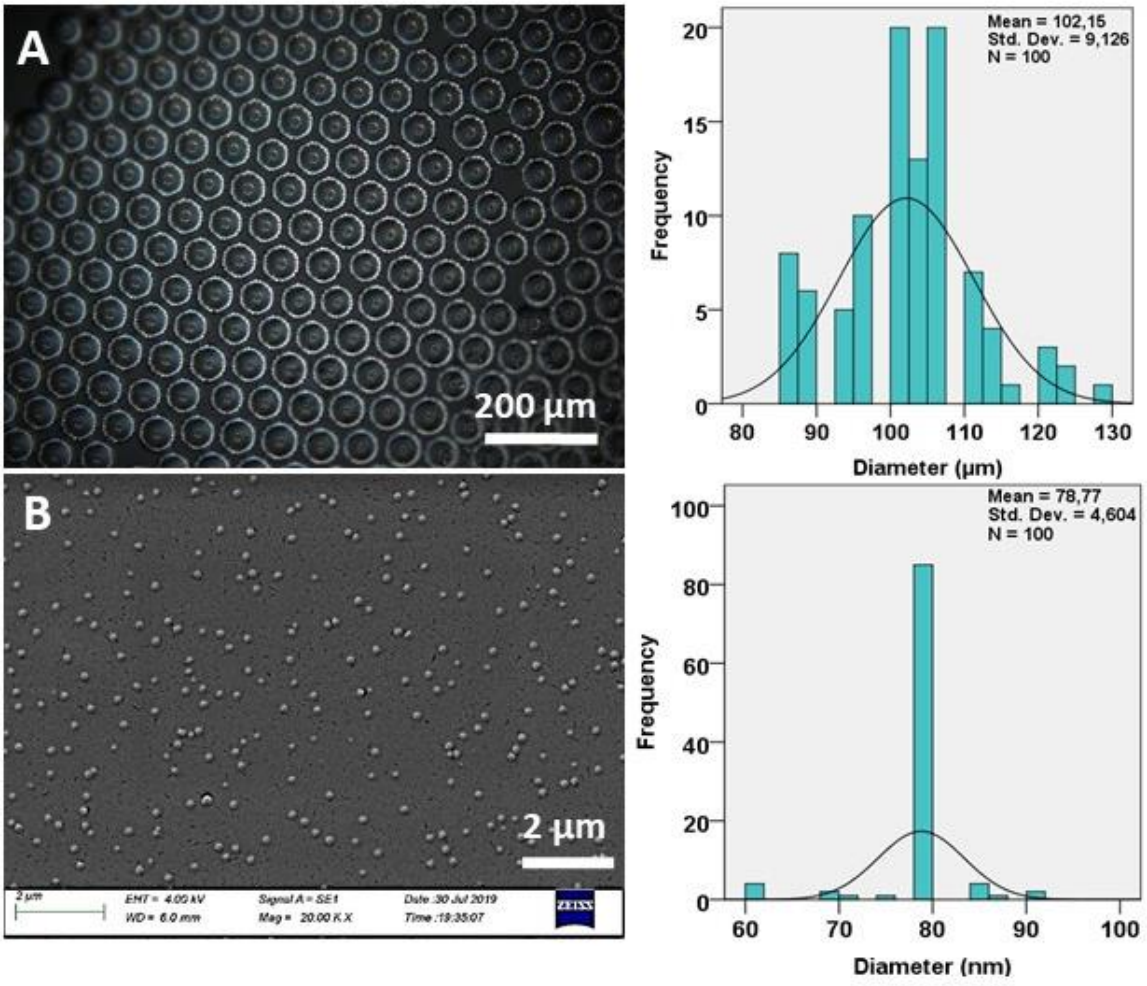
A
200 µm
B
2 µm
Mean = 102,15
Std. Dev. = 9,126
N = 100
Frequency
Diameter (µm)
Mean = 78,77
Std. Dev. = 4,604
N = 100
Frequency
Diameter (nm)

Figure 6

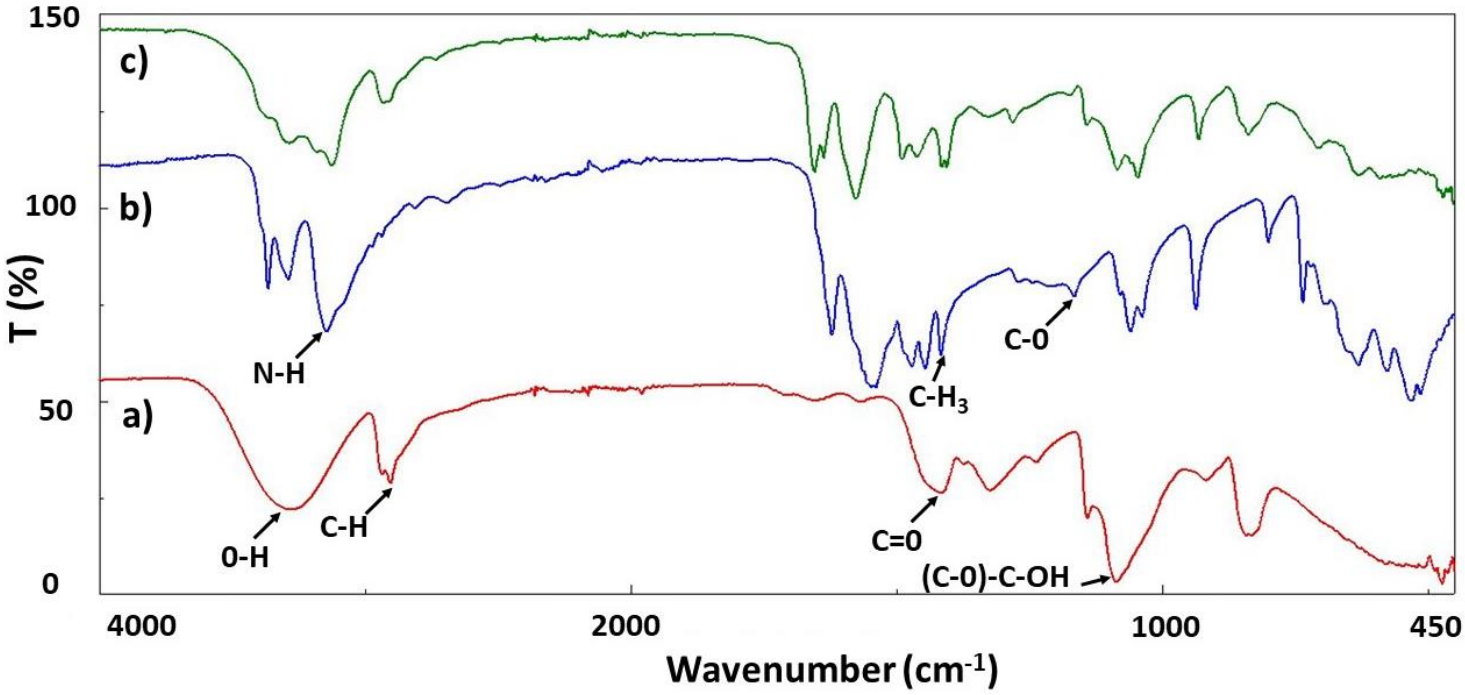
150
100
50
0
T (%)
c)
b)
a)
N-H
0-H
C-H
C=0
C-H3
C-0
(C-0)-C-OH
4000
2000
1000
450
Wavenumber (cm-1)

Figure 7

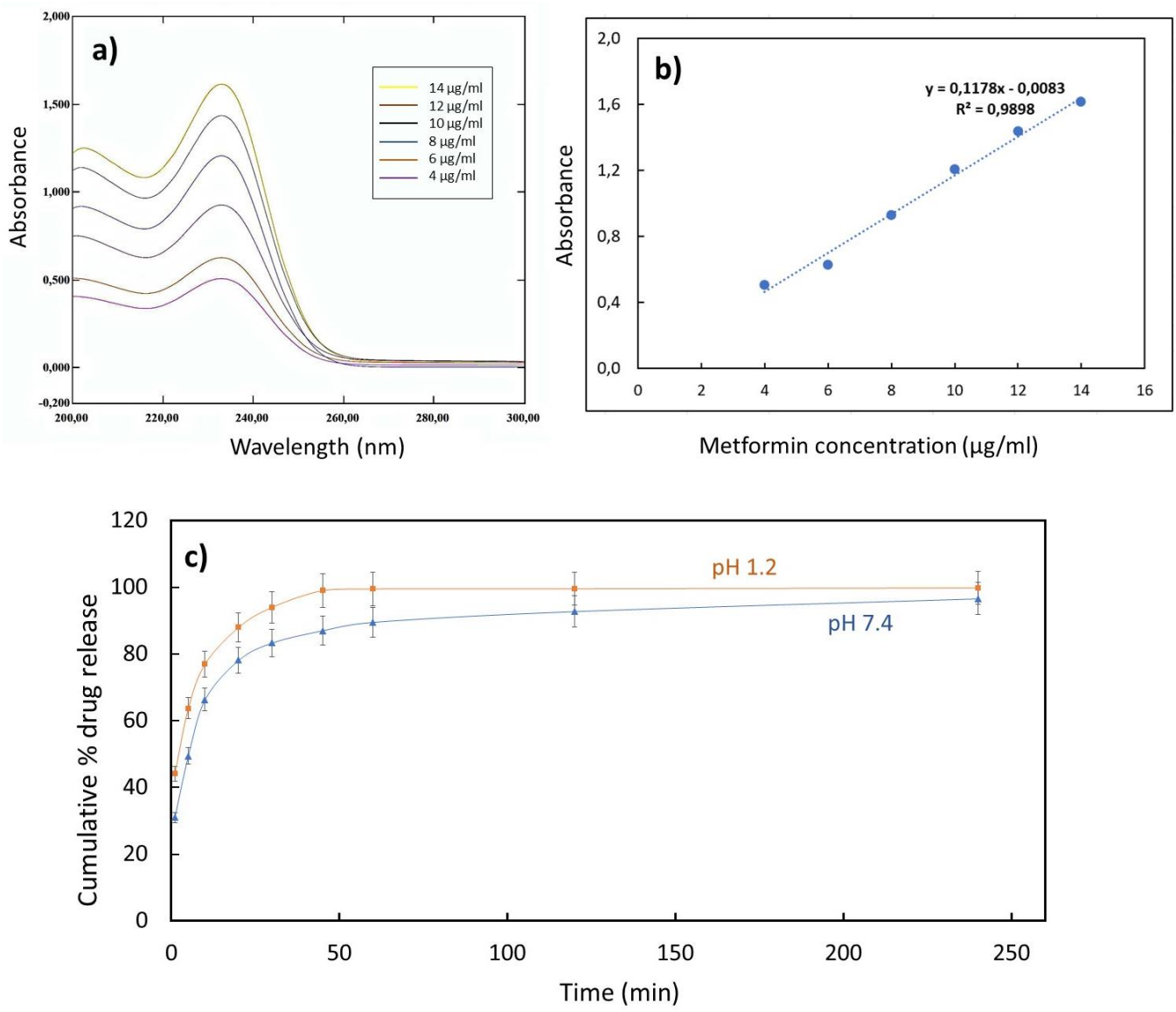
a)
Absorbance
Wavelength (nm)
14 µg/ml
12 µg/ml
10 µg/ml
8 µg/ml
6 µg/ml
4 µg/ml
b)
Absorbance
Metformin concentration (µg/ml)
y = 0,1178x - 0,0083
R² = 0,9898
c)
Cumulative % drug release
Time (min)
pH 1.2
pH 7.4

Figure 8

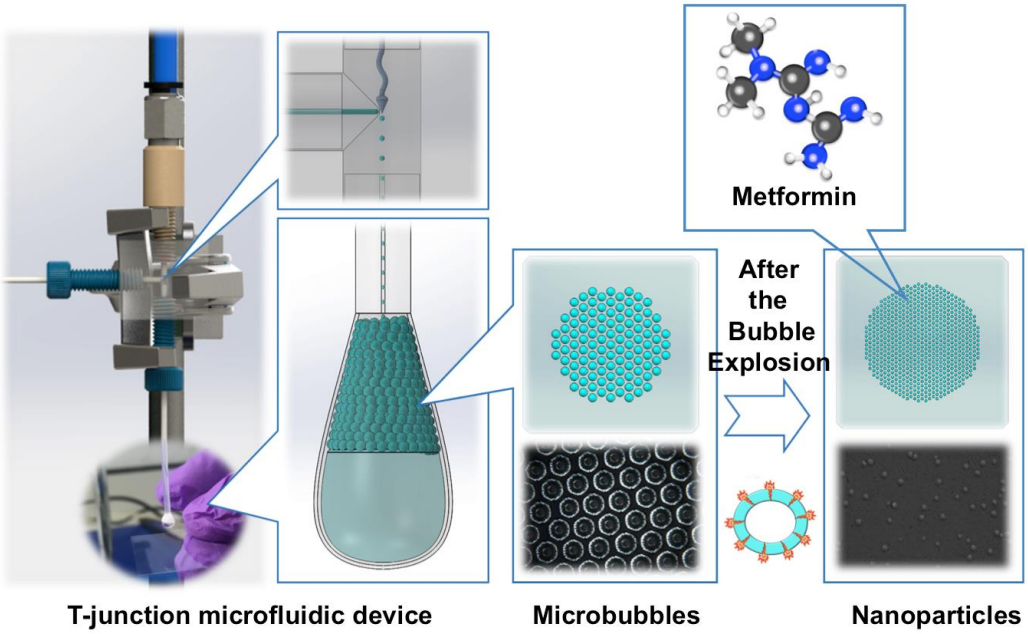
Metformin
After the Bubble Explosion
T-junction microfluidic device
Microbubbles
Nanoparticles

-TOC Graphic-